FUDMA Journal of Sciences (FJS)
ISSN: 2616-1370
Vol. 2 No. 1, April, 2018, pp 23-42

THERMO-DIFFUSION AND DIFFUSION-THERMO EFFECTS ON MIXED CONVECTION HYDROMAGNETIC FLOW IN A THIRD GRADE FLUID OVER A STRETCHING SURFACE IN A DARCY-FORCHHEIMER POROUS MEDIUM

[1]Baoku, I. G. and [2]Fadare, S. A.

[1]Department of Mathematical Sciences, Federal University, Dutsin-Ma, Katsina State, Nigeria.
[2]Department of Electrical/Electronics, Federal Polytechnics, Ilaro, Ogun State, Nigeria.

ABSTRACT
This paper is concerned with the influences of thermo-diffusion and diffusion-thermo on the mixed convection flow, heat and mass transfer of a viscoelastic third grade fluid along a vertical surface in a Darcy-Forchheimer porous medium. The surface is assumed to be permeable in the presence of thermal radiation, Joule heating, viscous dissipation, non-uniform heat source/sink and chemical reaction of order n. Adopting the equation for conservation of momentum for the third grade fluid, the basic boundary layer equations of heat and mass transfer, which are nonlinear partial differential equations, are converted into a system of coupled nonlinear ordinary differential equations by means of similarity transformations. Numerical solutions are obtained for the resulting boundary value problems by employing midpoint integration scheme enhanced by Richardson's extrapolation. The effects of various pertinent parameters are shown in several plots. Skin-friction coefficient, local Nusselt and Sherwood numbers are tabulated in order to gain more insight into the surface shear stress, rates of heat and mass transfer of the problem. Soret and Dufour numbers are found to be increasing functions of the species concentration and thermal boundary layer thicknesses respectively.

Keywords: Mixed convection, Thermo-diffusion, Diffusion-thermo, Hydromagnetic flow, Third grade fluid.
[1]Corresponding Author Email: ibaoku@fudutsinma.edu.ng

INTRODUCTION

It is obvious that many fluids that are commonly used for industrial processes differ greatly from the Newtonian behaviour in their rheology. Flows involving non-Newtonian fluids have been theoretically and experimentally studied due to their importance in numerous scientific and technological applications. Examples of non-Newtonian fluids are polymers, pulps, molten plastics, foods and slurries. Many different non-Newtonian fluid models have appeared in the literature to convey the deviation from the viscous fluids. One of the non-Newtonian fluid groups which has gained much attention of researchers is the differential type fluid. Fundamental applications of such fluids with heat and mass transfer are in heat exchangers, electronics cooling, screw extrusion process, and many others. Interesting reviews of differential type fluids are given by Khani *et al.* (2009), Fosdick and Rajagopal (1980) and Dunn and Rajagopal (1995). Among the differential type fluids, Rivlin-Ericksen fluid, second and third grade fluid models have been extensively used. Some of previous work on flow, heat and mass transfer of third grade fluids with different geometries are in the works of Rivlin and Ericksen (1955), Hayat *et al.* (2010a), Sahoo (2010), Sahoo and Poncet (2011), Hayat *et al.* (2010b), Hayat *et al.* (2011), Makinde and Chinyoka (2011), Abbasbandy and Hayat (2011), Aiyesimi *et al.* (2012), Aziz and Aziz (2012), Hayat *et al.* (2013a), Hayat *et al.* (2013b) and Baoku *et al.* (2013).

The effects of thermophysical and chemical properties of non-Newtonian fluid cannot be neglected while studying the non-Newtonian viscoelastic third grade fluids. The problem of heat transfer analysis was considered in electrically conducting thin film flows of a third grade on a vertical belt with slip boundary conditions by Gul *et al.* (2013). They employed optimal homotopy asymptotic method (OHAM) to obtain results for the profile of velocity, volume flux, skin-friction, average velocity and the temperature distribution across the film. Also, Gul *et al.* (2014) further carried out an investigation on the temperature-dependent viscosity on thin film flow of a magnetohydrodynamic (MHD) third grade fluid past a vertical belt and discussed the physical characteristics of the problem. The unsteady stagnation point boundary layer flow and heat transfer of a special third grade fluid past a permeable stretching/shrinking sheet was numerically investigated by Naganthran *et al.* (2016). They obtained dual solutions for both cases of stretching and shrinking sheet using the bvp 4c function in MATLAB. Poonia and Bhargava (2015) studied the heat and mass transfer in an unsteady boundary layer flow of an incompressible, laminar, natural convective, and temperature-dependent third grade fluid. They took into account the effect of viscous dissipation and variable suction.

Olajuwon and Baoku (2014) also analyzed the magnetohydrodynamic flow, heat and mass transfer of a viscoelastic third grade fluid with partial slip past an infinite porous plate with constant surface temperature in a porous medium. They concluded that the velocity and thermal boundary layer decreased with an increase in the partial slip. Hayat *et al.* (2011) discussed the effects of wall properties on the peristaltic flow of an incompressible third grade fluid in a curved channel. They obtained a series solution under the approximation of long wavelength and low Reynolds number. Hayat *et al.* (2010) also examined the unsteady flow with heat and mass transfer characteristics in a third grade fluid bounded by a stretching sheet using homotopy analysis method (HAM). Farooq *et al* (2014) examined the heat and mass transfer of two-layer flows on non-Newtonian third grade fluid in a channel when one layer of water was nanofluid and the other was clear with viscous dissipation. They found that the layer of nano-fluids had many different properties from that of clear fluid. Hayat *et al.* (2014) presented the analysis of mixed convection flow of incompressible third grade fluid over a porous and linearly stretching sheet in the presence of thermal stratified effects. The influence of thermophoresis and Brownian motion was considered in two-dimensional boundary

layer flow of an incompressible third grade nanofluid over a stretching surface in the presence of Newtonian heating and viscous dissipation by Shehzad *et al.* (2015). Nadeem and Saleem (2015) analytically studied the third grade fluid flow over a rotating vertical cone in the presence of nanoparticles and proffered solutions to the boundary layer momentum, energy and diffusion equation using HAM. Rashidi *et al.* (2015) also analyzed the convective flow of a third grade non-Newtonian fluid due to a linearly stretching sheet subject to a magnetic field. They established that the thermal boundary layer thickness decreased with increasing Prandtl number. Hayat *et al*. (2015) further focused on the analytic solution of steady boundary layer axisymmetric flow of third grade fluid over a continuously stretching cylinder in the presence of magnetic field. They found that velocity and momentum boundary layer thicknesses were increasing functions of curvature parameter. Analysis was carried out to study the entropy generation rate in the flow and heat transfer of hydromagnetic third grade fluid between horizontal parallel plates saturated with porous materials. The flow was induced by a constant pressure gradient applied in the flow direction and also influenced by a uniform magnetic field-applied across the flow channel. Abdulhameed *et al.* (2015) analyzed the unidirectional flow of an incompressible electrically conducting third-grade fluid past a vertical transpiration wall through a porous medium with time-dependent periodic motion. The buoyancy-induced flow of third grade nanofluids along a vertical permeable stretching sheet was examined by Khan *et al.* (2015). They obtained a numerical solution for the combined heat and mass transfer during convective cooling of the stretching sheet, subject to partial slip and convective solutal boundary conditions.

Recently, Imtiaz *et al.* (2017) presented the two-dimensional flow of third grade fluid induced by a linear stretching sheet while effects of chemical reaction were taken into consideration. They showed that increasing values of thermal relaxation time correspond to low temperature by using Cattaneo-Christov heat flux model. Hayat *et al.* (2018) examined the modeling and analyzing flow of a third-grade nanofluid due to rotating stretchable disk in the presence of chemical reaction and heat source. HAM was used to obtain solutions to induced flows of third-grade nanofluid along a vertical permeable stretching sheet. The problem of the two-dimensional mixed convection stagnation-point flow of a magnetohydrodynamic non-Newtonian third-grade nanofluid bounded by a vertical stretching sheet was considered by Golafshan and Rahimi (2018). They also considered work done due to deformation in their problem and discussed different physical parameters on the dynamics of the problem. Gaffar *et al.* (2018) analyzed the radiative and magnetohydrodynamic flow of a third-grade viscoelastic fluid past an isothermal inverted cone in the presence of heat generation/absorption. They gave detailed interpretation of the computations using the second-order accurate implicit finite-difference Keller-box method.

Following Fourier's and Fick's laws, many researchers neglect the Soret and Dufour effects (thermo-diffusion and diffusion-thermo effects respectively). However, when there are density differences in the flow mechanism, these effects cannot be neglected. The present work extends the model of third grade flow investigated by Khani *et al.* (2009) to involve mixed convective flow, heat and mass transfer. The flow regime, under investigation, incorporates viscous dissipation, Joule heating, thermal radiation, non-uniform heat generation/absorption and chemical reaction of order n while taken into account Soret and Dufour effects.

MATHEMATICAL FORMULATION OF THE PROBLEM

Consider the mixed convective flow, heat and mass transfer due to a vertical stretching surface embedded in a Darcy-Forchheimer porous medium filled with a viscoelastic third grade fluid. The heated vertical surface temperature is T_w and species concentration at the surface is C_w. The flow, which involves a n^{th} order chemically reacting third grade fluid, is subjected to a transversely uniform magnetic field in the presence of non-uniform heat generation/absorption, Joule heating, viscous dissipation and thermal radiation. Assuming other fluid properties are constant, the density variation and the buoyancy effects are taken into account so that the Boussinessq approximation for both the temperature and species concentration gradient is adopted. The fluid and solid matrix are assumed to be in a local thermal equilibrium and the magnetohydrodynamic behaviour is steady with the consideration for Soret and Dufour effects. In the case of negligible pressure gradient, the equation of motion [adopting Khani *et al.* (2009)], boundary layer equations of thermal and species concentration for the problem are given by the following coupled nonlinear differential equations as follows:

$$\mu\frac{d^2\bar{u}}{dy^2}-\alpha_1 V_0\frac{d^3\bar{u}}{dy^3}+\rho V_0\frac{d\bar{u}}{dy}+6\beta_3\left(\frac{d\bar{u}}{dy}\right)^2\frac{d^2\bar{u}}{dy^2}-\sigma B_0^2\bar{u}+\rho g\beta_T\left(T-T'_\infty\right)+\rho g\beta_C\left(C-C_\infty\right)=\frac{\mu}{k_p}\bar{u}+\frac{\rho b\bar{u}^2}{k_p} \quad (1)$$

$$\bar{u}\frac{\partial T}{\partial x}-V_0\frac{\partial T}{\partial y}=\frac{\kappa}{\rho C_p}\frac{\partial^2 T}{\partial y^2}-\frac{1}{\rho C_p}\frac{\partial q_r}{\partial y}+\frac{\mu}{\rho C_p}\left(\frac{\partial\bar{u}}{\partial y}\right)^2+\frac{2\beta_3}{\rho C_p}\left(\frac{\partial\bar{u}}{\partial y}\right)^4+\frac{q'''}{\rho C_p}+\frac{\sigma B_0^2}{\rho C_p}\bar{u}^2+\frac{D_e k_T}{C_s C_p}\frac{\partial^2 C}{\partial y^2} \quad (2)$$

$$\bar{u}\frac{\partial C}{\partial x}-V_0\frac{\partial C}{\partial y}=D_B\frac{\partial^2 C}{\partial y^2}-k_1\left(C-C_\infty\right)^n+\frac{D_e K_T}{T_m}\frac{\partial^2 T}{\partial y^2} \quad (3)$$

Following Fosdick and Rajagopal (1980) in equation (1), the appropriate boundary conditions at the surface and in the free stream for the problem are:

$$\bar{u} = \bar{u}_w(x) = ax, \quad v = -V_0, \qquad T = T_w, \quad C = C_w \quad \text{at } y = 0 \tag{4}$$

$$\bar{u} \to 0, \ \frac{d\bar{u}}{dy} \to 0, \ T \to T_\infty, \qquad C \to C'_\infty \qquad \text{as } y' \to \infty \tag{5}$$

where a $(a > 0)$ is a constant. It should be noted that $v = -V_0$ where $V_0 > 0$ represents suction, i.e. lateral mass flux into the flow field and $V_0 < 0$ denotes blowing , i.e. mass removal from the flow field. Following Prasad *et al.* (2000), the space and temperature dependent internal heat generation/absorption (non-uniform heat source or sink) can be expressed in simplest form as:

$$q''' = \left(\frac{\kappa \bar{u}_w(x)}{x\nu}\right)\left[A^*(T_w - T'_\infty)\frac{d\bar{u}}{dy} + B^*(T - T'_\infty)\right] \tag{6}$$

where A^* and B^* are parameters of the space and temperature dependent internal heat generation/absorption.
Also, the radiative heat flux for optically thick environment with a non-linearized Rosseland approximation employed by Sparrow and Cess (1995) is adopted as: $q' = \dfrac{-4\sigma^*}{3\xi}\dfrac{\partial T^4}{\partial y}$ (7)

where σ^* is the Stefan-Boltzmann constant and ξ is the mean absorption coefficient.

Using the following similarity transformation: $\eta = \dfrac{ay\rho}{\mu}$, $u = \dfrac{\bar{u}}{a}$, $\theta = \dfrac{T - T_\infty}{T_w - T_\infty}$, $\phi = \dfrac{C - C_\infty}{C_w - C_\infty}$ (8)

in addition to (6), (7) and (8), equations (1) – (3) reduce to the following highly coupled nonlinear ordinary differential equations:

$$\frac{d^2u}{d\eta^2} - \alpha\frac{d^3u}{d\eta^3} + w\frac{du}{d\eta} + \beta\left(\frac{du}{d\eta}\right)^2\frac{d^2u}{d\eta^2} - \left(M + D + D_f u\right)u + \lambda\left(\theta + N\phi\right) = 0 \tag{9}$$

$$\left[1 + \frac{4Rd}{3}\left(\theta + Cr\right)^3\right]\frac{d^2\theta}{d\eta^2} + 4Rd\left(\theta + Cr\right)^2\left(\frac{d\theta}{d\eta}\right)^2 + \frac{1}{3}\beta\,\mathrm{Pr}\,Ec\left(\frac{du}{d\eta}\right)^2 + A\frac{du}{d\eta} + B\theta + M\,\mathrm{Pr}\,Ec\,u^2 + w\,\mathrm{Pr}\frac{d\theta}{d\eta} + Du\frac{d^2\phi}{d\eta^2} = 0 \tag{10}$$

$$\frac{d^2\phi}{d\eta^2} + \mathrm{Pr}\,Le\left(w\frac{d\phi}{d\eta} - Kr\,\phi^n\right) + Sr\frac{d^2\theta}{d\eta^2} = 0 \tag{11}$$

The boundary conditions are transformed as:

$$u(\eta) = S, \ \theta(\eta) = 1, \ \phi(\eta) = 1 \text{ at } \eta = 0 \tag{12}$$

$$u(\eta) \to 1, \frac{du}{dy}(\eta) \to 0, \ \theta(\eta) \to 0,$$

$$\phi(\eta) \to 0 \qquad \text{as } \eta \to \infty \tag{13}$$

where S is the stretching rate of the surface, $\alpha = \dfrac{\rho\alpha_1 a^2}{\mu^2}\cdot w$, $\beta = \dfrac{6\beta_3\rho a^2}{\mu^2}$, $M = \dfrac{\sigma B_0^2 \nu}{a^2\rho}$, $D = \dfrac{\mu^2}{a^2\rho^2 k_p}$,

$Df = \dfrac{\mu b}{a\rho k_p}$, $\lambda = \dfrac{Gr_x}{\mathrm{Re}_x^2}$, $Le = \dfrac{\alpha}{D_B}$, $\mathrm{Re}_x^2 = \dfrac{a^2x^2}{\nu^2}$, $N = \dfrac{\beta_C(C_w - C_\infty)}{\beta_T(T_w - T_\infty)}$,

$$Rd = \frac{4\sigma^*(T_w - T_\infty)^3}{a_R k_c}, Cr = \frac{T_\infty}{T_w - T_\infty}, \Pr = \frac{\nu}{\alpha_m}, w = \frac{V_0}{a}, Du = \frac{D_e K_T (C_w - C_\infty)}{\alpha C_s C_p (T_w - T_\infty)},$$

$$Sr = \frac{K_T (T_w - T_\infty)}{T_m (C_w - C_\infty)}, Gr_x = \frac{g\beta_T (T_w - T_\infty)\nu}{a^3}, \quad Ec = \frac{U_\infty^2}{C_p (T_w - T_\infty)}.$$

METHOD OF SOLUTION

The system of coupled nonlinear differential equations (9) – (11) together with the boundary conditions (12) and (13) have been solved numerically by midpoint integration technique with Richardson's extrapolation. The method creates higher order accurate approximations and prevents grid dependence on the results obtained. It should be noted that the order of the system of differential equations corresponds to the number of adherent boundary conditions. Thus, the system of equations is well-posed and the boundary conditions are sufficient to facilitate the computations. The algorithm of the numerical technique is such that the given system of equations alongside the boundary conditions is converted into first order coupled ordinary nonlinear differential equations. Replacing the semi-infinite integration domain $\eta \in [0, \infty)$ with a finite domain $\eta \in [0, \eta_\infty]$. The modified Newton's iteration technique is further employed as a suitable algorithm to pinpoint the values of solutions at the finite domain.

Thus, the numerical procedural computations have been performed by a program which uses a symbolic and computational computer language MAPLE as described by Heck (2003). A mesh spacing of $\Delta\eta = 0.001$ has been selected to sufficiently achieve a convergence criterion of 10^{-7} in all cases. Using an assignment statement $\eta_\infty = \eta_\infty + \Delta\eta$, the value of η_∞ is found to each iteration loop. Hence, the numerical technique has been employed to obtain required solutions for the emerging parameters: β, α, M, Rd, Cr, $\Pr$, Ec, A, B, Df, Du, Sr, N, λ and others. The accuracy of this algorithm is hiked to $O[(\Delta\eta)^6]$ by invoking Richardson's extrapolation.

RESULTS AND DISCUSSION

An analysis is carried out to investigate the Soret and Dufour effects on heat and mass transfer of a viscoelastic third grade fluid in a mixed convection boundary layer MHD flow embedded in a Darcy-Forchheimer porous medium in presence of viscous dissipation, Joule heating, non-uniform heat generation/absorption, thermal radiation and chemical reaction of order n. The nonlinear coupled boundary value problem consisting of equations (9) - (11) with conditions (12) - (13) is solved numerically by assigning realistic numerical values to the embedded parameters in the system of equations. This is done in order to gain an insight into the flow structure with respect to velocity, temperature and species concentrations profiles. In the computations, the variations of velocity u, temperature θ and species concentration ϕ versus η for the respective velocity, temperature and species concentration boundary layers are desired.

Velocity Profiles

Figures 1-16 show the influences of emerging flow parameters on dimensionless velocity profiles. Figure 1 depicts the effect of viscoelastic third grade material parameter on the velocity profile. It is found that an increase in the viscoelastic third grade material parameter enhances the velocity profile. This observation is similar to that of Khani *et al.* (2009). The viscoelastic second grade material parameter α shows the influence of the normal stress coefficient on the velocity profile. In this case, increasing the normal stress coefficient implies that the boundary layer thickness is increased. It is observed in Figure 2 that increasing the viscoelastic second grade material parameter suppresses the velocity profile which resulted into velocity boundary layer thinning. Figure 3 displays the solution of velocity profile across the boundary layer for different values of magnetic interaction parameter M. It is observed that increasing the value of M leads to an increasing in the fluid velocity.

Figures 4 and 5 demonstrate the effects of space dependent and temperature dependent internal heat source/sink, A and B respectively on the velocity profile. Velocity profile is enhanced for space internal heat generation/absorption while it is suppressed for temperature dependent internal heat generation/absorption. It is interesting to note that the velocity profile is influenced by the temperature difference parameter Cr which is not always the case in an optically thin environment. Figure 6 elucidates this fact and it is found that an increase in Cr increases the velocity distribution. Similarly, the effect of order of chemical reaction n is shown in Figure 7. The velocity profile is equally observed to increase as the value order of chemical reaction parameter increases.

In the same vein, the Eckert number Ec, which is used to characterize heat dissipation, has noticeable influence on the velocity profile. An increase in Ec is observed to enhance the velocity distribution in Figure 8. Figure 9 illustrates the effect of Forchheimer parameter Df on the velocity profile. An increase in the velocity profile is noticed with increasing values of Df. Figures 10 and 11 show the variation of velocity profiles for different values of transpiration w and Darcian porous medium Pm parameters respectively. Both physical parameters are observed to have enhanced the velocity profiles as their values increase. The influence of suction velocity parameter S is displayed in Figure 12. An increase in the velocity profile is noticed as the values of S increases. Figures 13 and 14 reveal that the dimensionless concentration buoyancy N and mixed convection λ parameters have the

same effects on the velocity distribution. They both depress the velocity profiles thereby increasing the velocity boundary layer thicknesses. Similarly, Figures 15 and 16 express the variations of Prandtl $\Pr$ and Dufour Du numbers respectively. They are found to be decreasing functions of the velocity profiles.

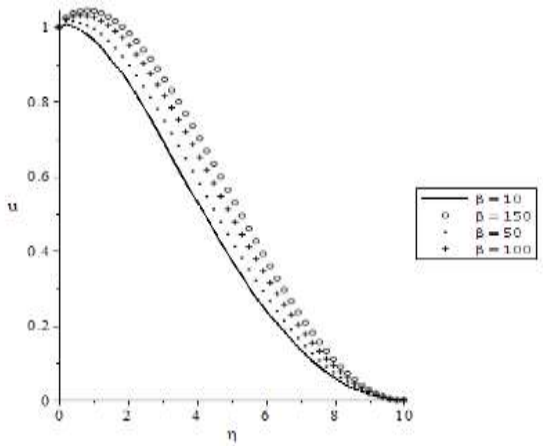

Figure 1: Effect of β on velocity profile when $\alpha = 50,\ M = 0.5,\ \lambda = 0.2,\ w = 0.001,\ Pm = 0.5,\ Df = 1.5,\ N = -2.$

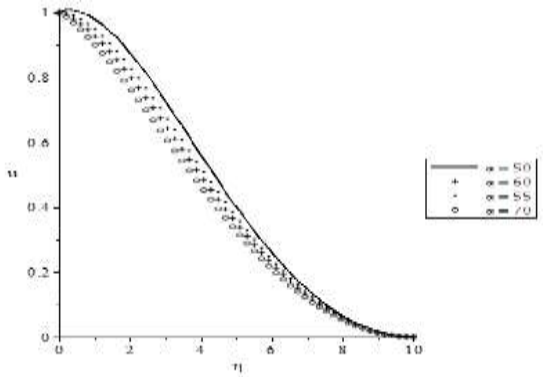

Figure 2: Effect of α on velocity profile when $\beta = 30,\ M = 0.5,\ \lambda = 0.2,\ w = 0.001,\ Pm = 0.5,\ Df = 1.5,\ N = -2.$

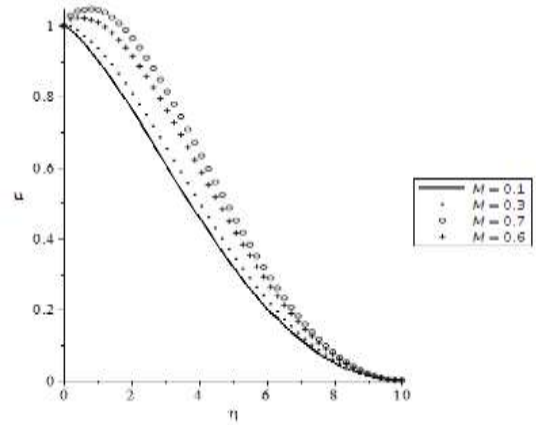

Figure 3: Effect of M on velocity profile when $\alpha = 50,\ \beta = 30,\ \lambda = 0.2,\ w = 0.001,\ Pm = 0.5,\ Df = 1.5,\ N = -2.$

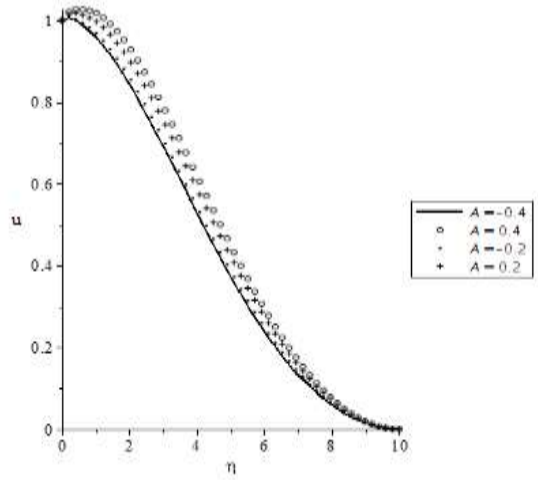

Figure 4: Effect of A on velocity profile when $\alpha = 50,\ M = 0.5,\ \lambda = 0.2,\ w = 0.001,\ Pm = 0.5,\ \beta = 30,$ $Df = 1.5,\ N = -2.$

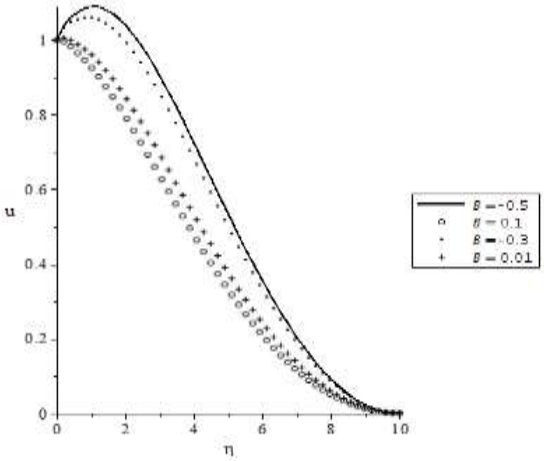

Figure 5: Effect of B on velocity profile when $\alpha = 50,\ M = 0.5,\ \lambda = 0.2,\ w = 0.001,\ Pm = 0.5,\ \beta = 30,$ $Df = 1.5,\ N = -2.$

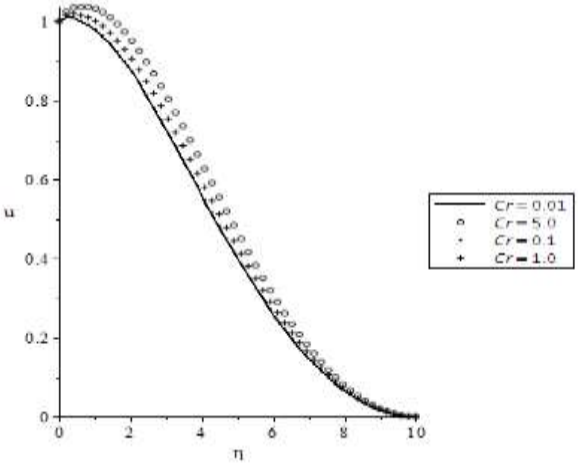

Figure 6: Effect of Cr on velocity profile when $\alpha = 50,\ M = 0.5,\ \lambda = 0.2,\ w = 0.001,\ Pm = 0.5,\ \beta = 30,$ $Df = 1.5,\ N = -2.$

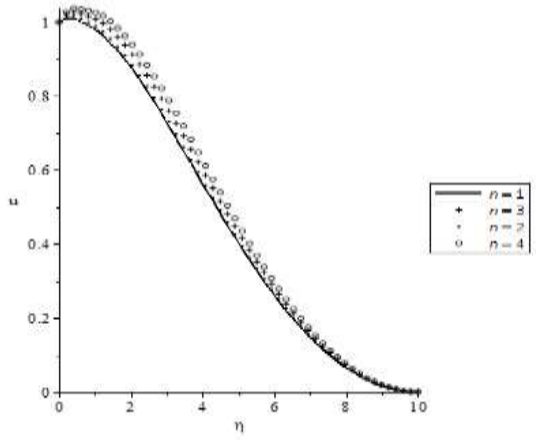

Figure 7: Effect of n on velocity profile when $\alpha = 50,\ M = 0.5,\ \lambda = 0.2,\ w = 0.001,\ Pm = 0.5,\ \beta = 30,$ $Df = 1.5,\ N = -2.$

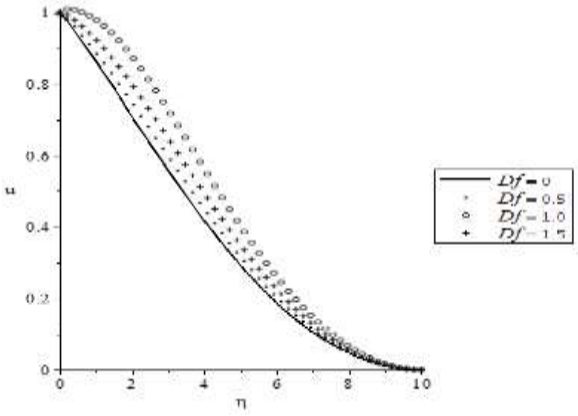

Figure 9: Effect of Df on velocity profile when $\alpha = 50,\ M = 0.5,\ \lambda = 0.2,\ w = 0.001,\ Pm = 0.5,\ \beta = 30,$ $N = -2.$

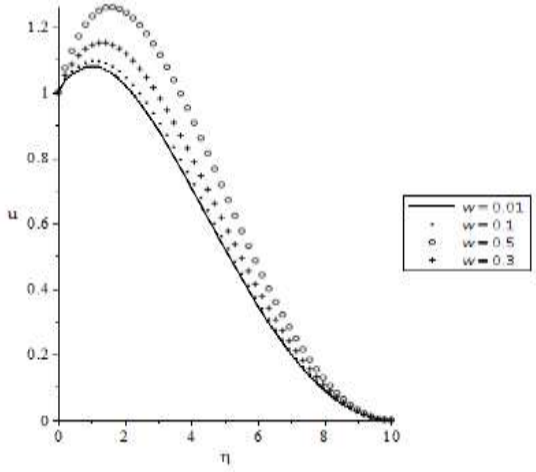

Figure 10: Effect of w on velocity profile when $\alpha = 50,\ M = 0.5,\ \lambda = 0.2,\ Pm = 0.5,\ \beta = 30,\ Df = 1.5,$ $N = -2.$

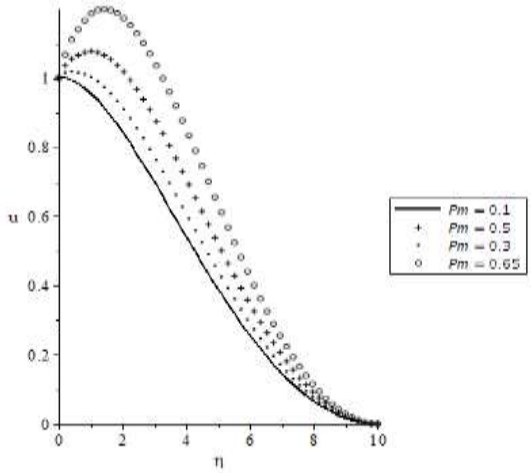

Figure 11: Effect of Pm on velocity profile when $\alpha = 50,\ M = 0.5,\ \lambda = 0.2,\ w = 0.001,\ \beta = 30,\ Df = 1.5,\ N = -2.$

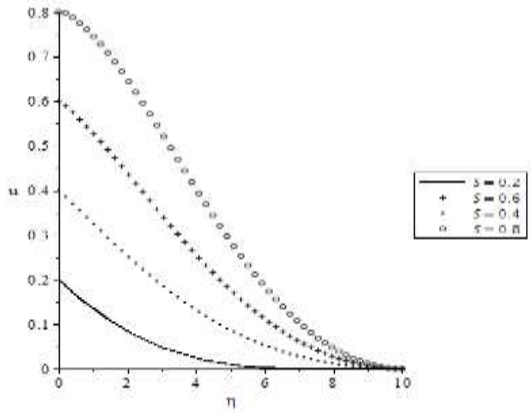

Figure 12: Effect of S on velocity profile when $\alpha = 50,\ M = 0.5,\ \lambda = 0.2,\ w = 0.001,\ Pm = 0.5,\ \beta = 30,\ Df = 1.5,\ N = -2.$

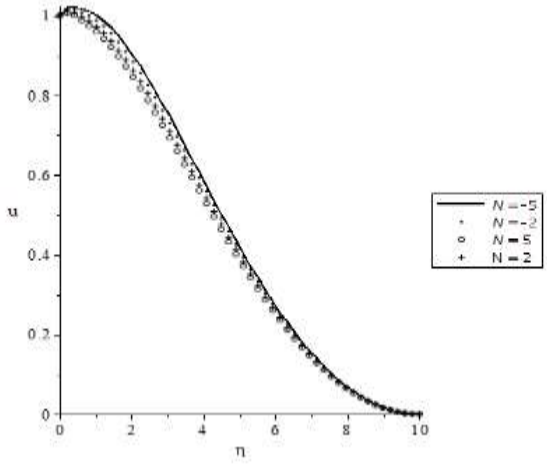

Figure 13: Effect of N on velocity profile when $\alpha = 50,\ M = 0.5,\ \lambda = 0.2,\ w = 0.001,\ Pm = 0.5,\ \beta = 30,\ Df = 1.5.$

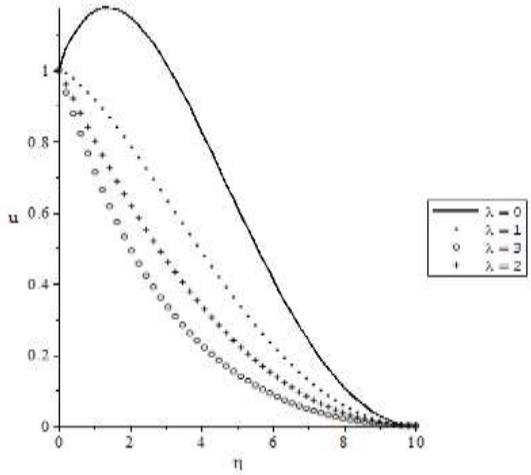

Figure 14: Effect of λ on velocity profile when $\alpha = 50,\ M = 0.5,\ w = 0.001,\ Pm = 0.5,\ \beta = 30,\ Df = 1.5,\ N = -2.$

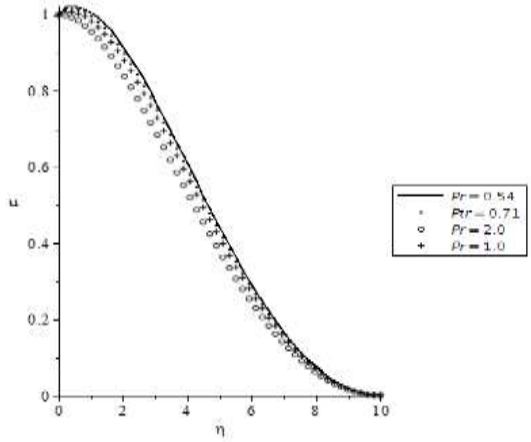

Figure 15: Effect of $\Pr$ on velocity profile when $\alpha = 50,\ M = 0.5,\ \lambda = 0.2,\ w = 0.001,\ Pm = 0.5,\ \beta = 30,\ Df = 1.5,\ N = -2.$

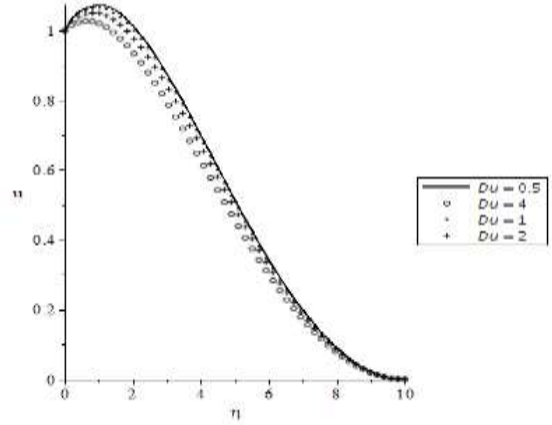

Figure 16: Effect of Du on velocity profile when $\alpha = 50,\ M = 0.5,\ \lambda = 0.2,\ w = 0.001,\ Pm = 0.5,\ \beta = 30,\ Df = 1.5,\ N = -2.$

Temperature Profiles

Figures 17-30 illustrate the influences of pertinent parameters in the flow field on the dimensionless temperature profiles. Figure 17 displays the variation of viscoelastic third grade material parameter β on the velocity profile. The thermal boundary layer thickness is enhanced by the increasing values

of β while other flow parameters are kept constant. This observation is in consonant with that of Khani *et al.* (2009). The effect of the viscoelastic second grade materials parameter α on the temperature profile is illustrated in Figure 18. In contrast to β, the thermal boundary layer thickness is depressed by the increasing values of α. Figures 19 and 20 depict the effects of temperature difference Cr and thermal radiation Rd parameters on the temperature distribution across the thermal boundary layer. The consequence of increasing the values of Cr decreases the fluid temperature. In the same vein, an increase in the values of Rd initially reduces the fluid temperature thereby reducing the thickness of the thermal boundary layer. This is expected because the effect of Rd is to reduce the temperature significantly in the flow region. Thermal radiation is found to be energy transfer by the emission of electromagnetic waves which carry energy away from the fluid flows. However, at the free stream, the effect of Rd on the thermal boundary layer is totally opposite.

Figures 21 and 22 have been portrayed to show the effects of space and temperature dependent heat source/sink A and B respectively. Unlike the influence of A and B on the momentum boundary layer for both values of $A>0$ and $B>0$ with $A<0$ and $B<0$, the thermal boundary layer thickness is enhanced with increasing values of B while it is depressed with increasing values of A. For the temperature-dependent heat source/sink parameter's enhancement of temperature profile, this implies that energy is released for increasing values of B which causes the increase in fluid temperature. However, in the case of the space dependent heat source/sink which depresses the thermal boundary layer. It corresponds to the case where boundary layer absorbs energy resulting in the temperature fall. It is worth mentioning to note that an increase in the magnetic interaction parameter M enhances the thermal boundary layer thickness as shown in Figure 23. Figure 24 shows the effect of Forchheimer parameter Df on the temperature distribution. The dimensionless temperature increases with increasing values of Forchheimer parameter. This observation is contrary to that of Khani *et al.* (2009). Inclusion of more virgin thermophysical parameters into the problem might be responsible for the different thermal boundary layer thicknesses.

In Figure 25, the order of chemical reaction parameter n influences the temperature profile. It is observed that increasing values of n slightly enhance the thermal boundary layer. The effects of dimensionless concentration buoyancy N and mixed convection λ parameters are illustrated by Figures 26 and 27 respectively. It is observed that both parameters depress the thermal boundary layer thicknesses. Figure 28 projects the influence of Eckert number Ec on the temperature profile. An increase in Ec corresponds to a significant increase in heat dissipation and hence, this increase the thermal boundary layer thickness. In Figure 29, the dimensionless Darcian porous medium parameter Pm is illustrated to reveal its effect on the temperature profile. It is observed that increasing values of Pm enhances the fluid temperature. This observation is in agreement with that of Khani *et al.* (2009). Figure 30 presents the effect of Prandtl number $\Pr$ on the temperature profile. It is found that an increase in the value of $\Pr$ enhances the thermal boundary layer thickness. Finally, the solution of the temperature profile for various values of the dimensionless Dufour number Du is displayed in Figure 31. As the Dufour number increases, it increases the thermal boundary layer throughout the η regime.

Species Concentration Profiles

The effects of embedded parameters on the species concentration profile are discussed in Figures 32-36. It is obvious that the influence of the chemical reaction parameter Kr is displayed in Figure 32. It shows that increasing Kr depresses the species concentration boundary layer thickness. Figures 33 and 34 show that the effects of Prandtl $\Pr$ and Lewis Le numbers on the species concentration profiles are similar. An increase in the values of $\Pr$ and Le corresponds to a decrease in the species concentration. Figure 35 shows that an increase in the order of chemical reaction parameter n corresponds to an increase the species concentration boundary layer thickness. Finally, the influence of Soret number on the species concentration distribution is displayed in Figure 36. Increasing the Soret number corresponds to an increase in the species concentration boundary layer thickness. It worth mentioning that observations on the behaviour of Dufour and Soret numbers are the same on the temperature and species concentration profiles respectively.

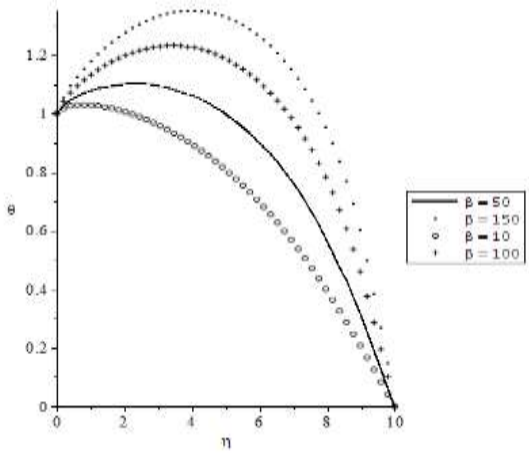

Figure 17: Effects of β on temperature profile when $Rd = 1.0,\ A = -0.01,\ B = -0.01,\ \Pr = 0.5,$ $Df = 1.5,\ Cr = 0.1,\ Ec = 0.2,\ Du = 0.1.$

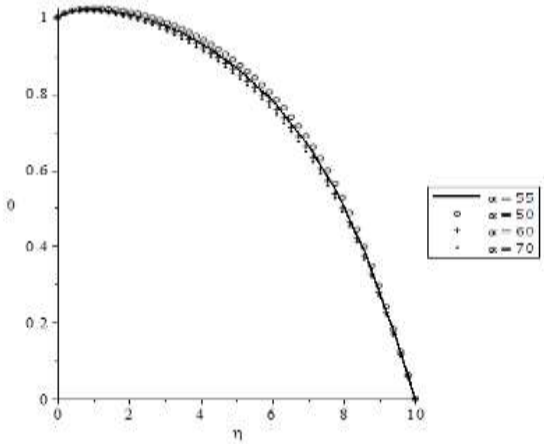

Figure 18: Effects of α on temperature profile when $Rd = 1.0,\ A = -0.01,\ B = -0.01,\ \Pr = 0.5,\ Df = 1.5,$ $Cr = 0.1,\ Ec = 0.2,\ Du = 0.1.$

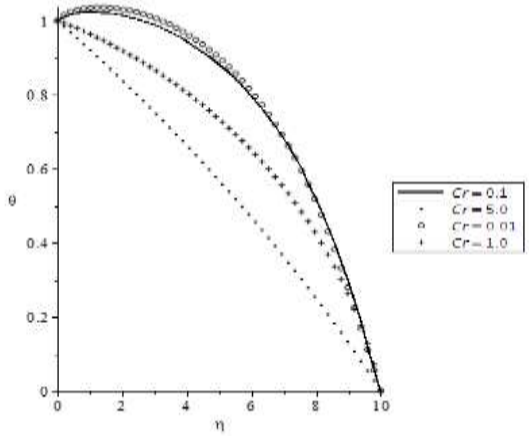

Figure 19: Effects of Cr on temperature profile when $Rd = 1.0,\ A = -0.01,\ B = -0.01,\ \Pr = 0.5,\ Df = 1.5,$ $Ec = 0.2,\ Du = 0.1.$

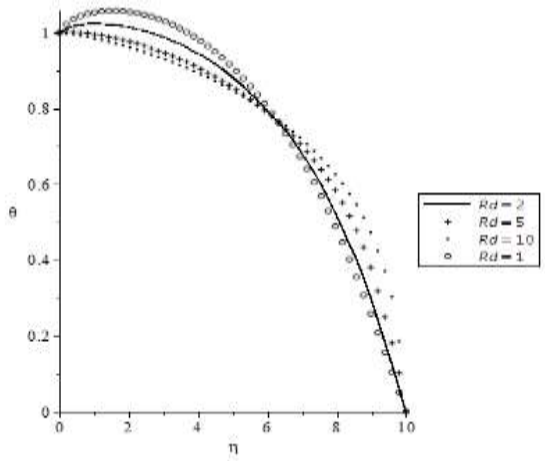

Figure 20: Effects of Rd on temperature profile when $A = -0.01,\ B = -0.01,\ \Pr = 0.5,\ Df = 1.5,\ Cr = 0.1,$ $Ec = 0.2, Du = 0.1.$

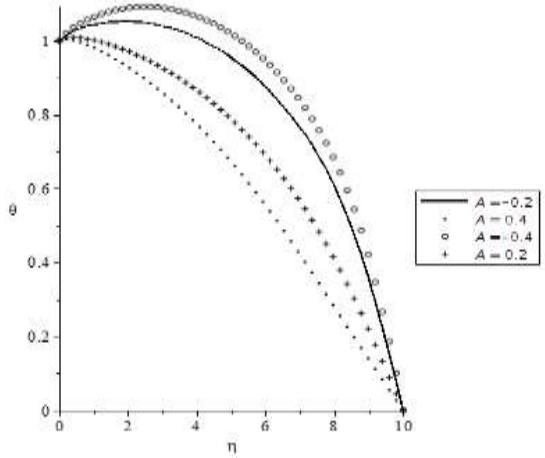

Figure 21: Effects of A on temperature profile when $Rd = 1.0,\ B = -0.01,\ \Pr = 0.5,\ Df = 1.5,\ Cr = 0.1,$ $Ec = 0.2, Du = 0.1.$

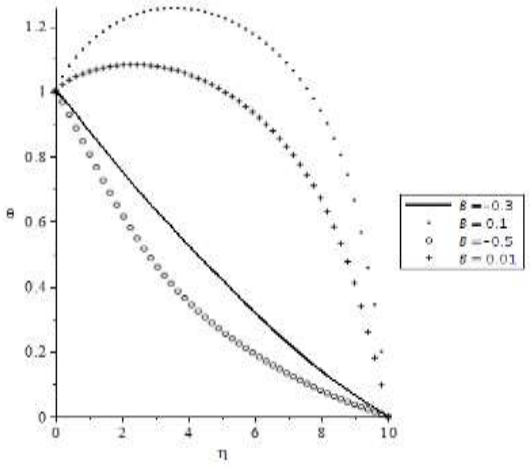

Figure 22: Effects of B on temperature profile when $Rd = 1.0,\ A = -0.01,\ \Pr = 0.5,\ Df = 1.5,\ Cr = 0.1,$ $Ec = 0.2, Du = 0.1.$

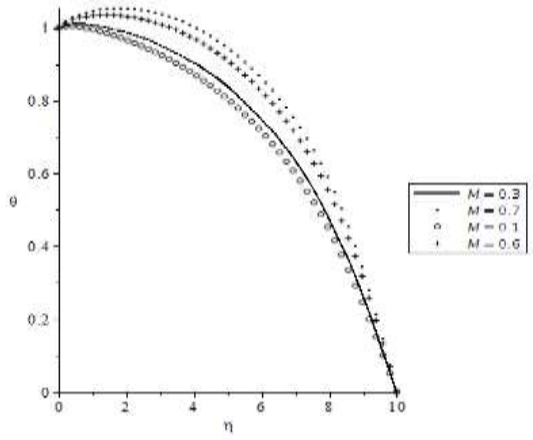

Figure 23: Effects of M on temperature profile when $Rd = 1.0,\ A = -0.01,\ Df = 1.5,\ Cr = 0.1,$ $Ec = 0.2, Du = 0.1$

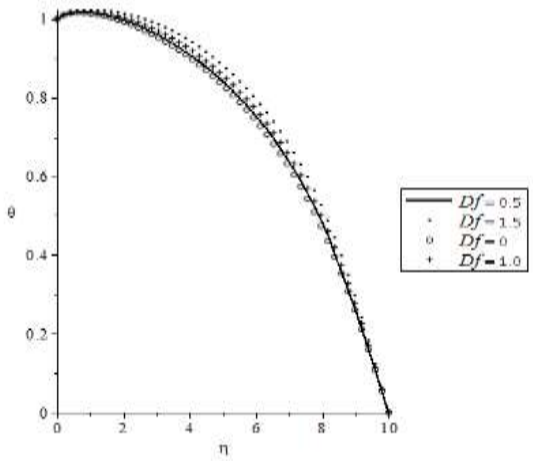

Figure 24: Effects of Df on temperature profile when $Rd = 1.0,\ A = -0.01,\ B = -0.01,\ \Pr = 0.5,\ Cr = 0.1,$ $Ec = 0.2,\ Du = 0.1.$

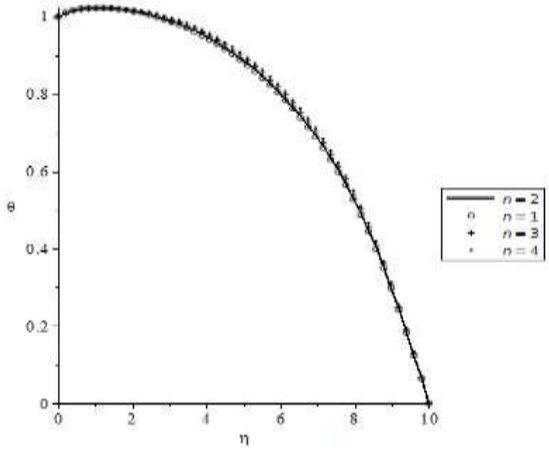

Figure 25: Effects of n on temperature profile when $Rd = 1.0,\ A = -0.01,\ B = -0.01,\ \Pr = 0.5,\ \ Df = 1.5,$ $Cr = 0.1,\ Ec = 0.2, Du = 0.1.$

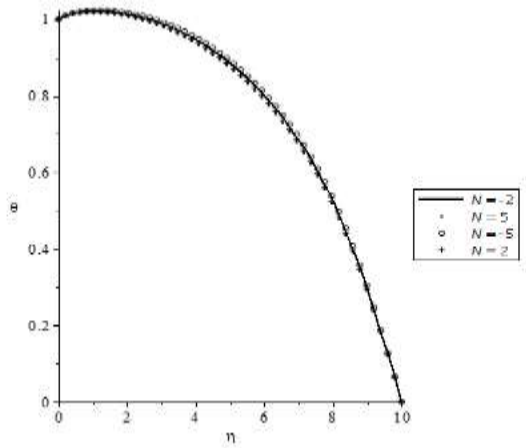

Figure 26: Effects of N on temperature profile when $Rd = 1.0,\ A = -0.01,\ B = -0.01,\ \Pr = 0.5,\ Df = 1.5,$ $Cr = 0.1,\ Ec = 0.2, Du = 0.1.$

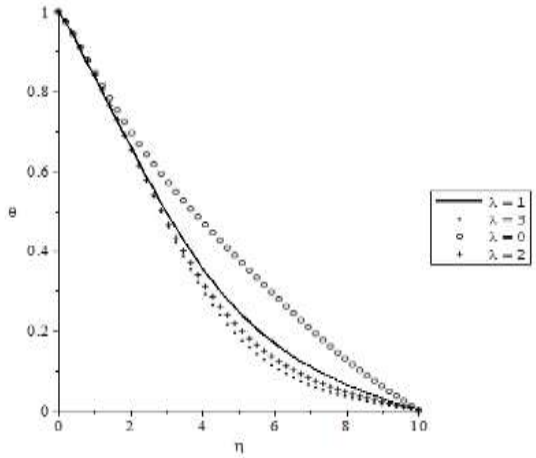

Figure 27: Effects of λ on temperature profile when $Rd = 1.0,\ A = -0.01,\ B = -0.01,\ \Pr = 0.5,\quad Df = 1.5,$ $Cr = 0.1,\ Ec = 0.2, Du = 0.1.$

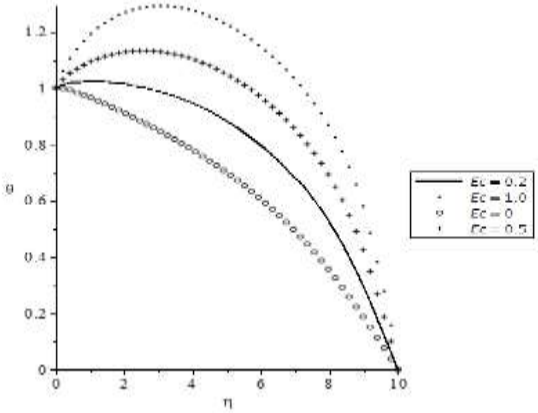

Figure 28: Effects of Ec on temperature profile when $Rd = 1.0,\ A = -0.01,\ B = -0.01,\ \Pr = 0.5, Df = 1.5,$ $Cr = 0.1, Du = 0.1.$

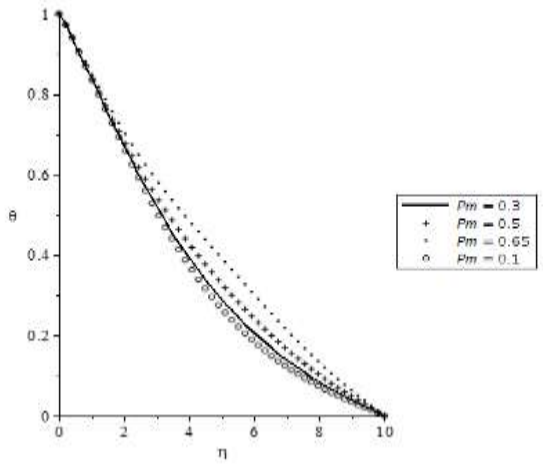

Figure 29: Effects of Ec on temperature profile when $Rd = 1.0,\ A = -0.01,\ B = -0.01,$ $\Pr = 0.5, Cr = 0.1, Ec = 0.2, Du = 0.1$.

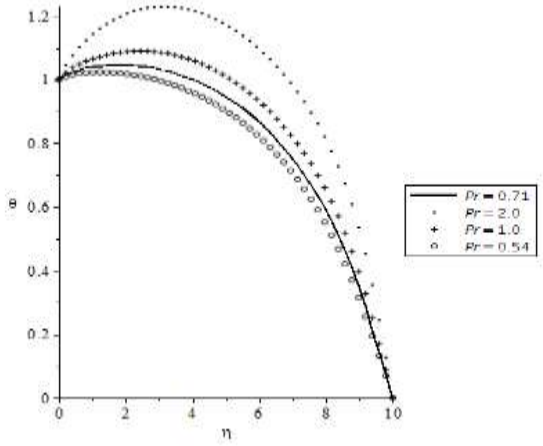

Figure 30: Effects of Ec on temperature profile when $Rd = 1.0,\ A = -0.01,\ B = -0.01,\ Df = 1.5,$ $Cr = 0.1, Ec = 0.2, Du = 0.1$.

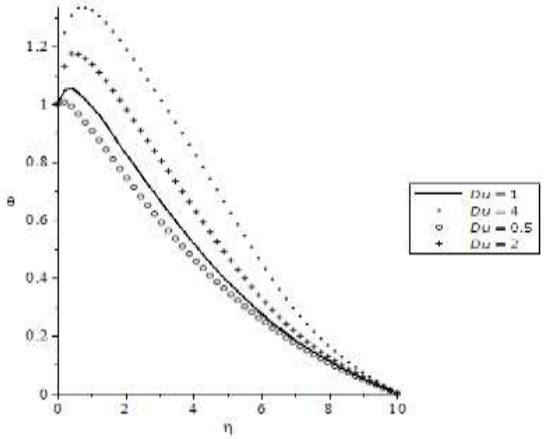

Figure 31: Effects of Ec on temperature profile when $Rd = 1.0,\ A = -0.01,\ B = -0.01,\ \Pr = 0.5, Df = 1.5,$ $Cr = 0.1, Ec = 0.2$.

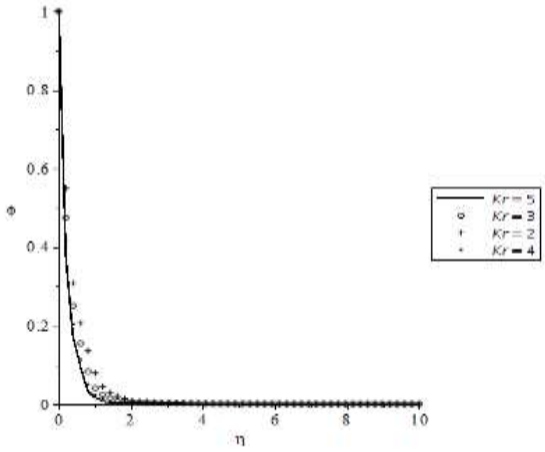

Figure 32: Effects of Kr on concentration profile when $n=1,\ Sr=0.1,\ w=0.001,\ \Pr=0.71,\ Le=2.816901$.

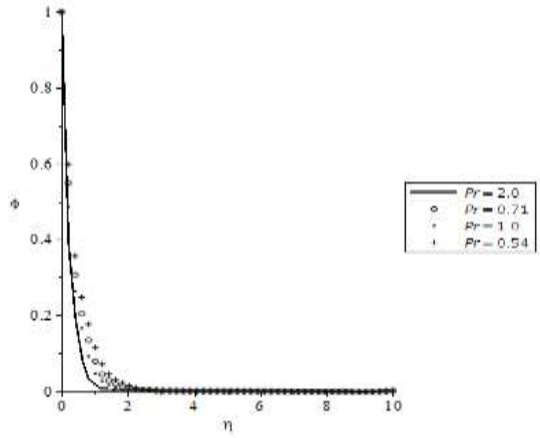

Figure 33: Effects of $\Pr$ on concentration profile when $n=1,\ Sr=0.1,\ w=0.001,\ Le=2.816901,\ Kr=2$.

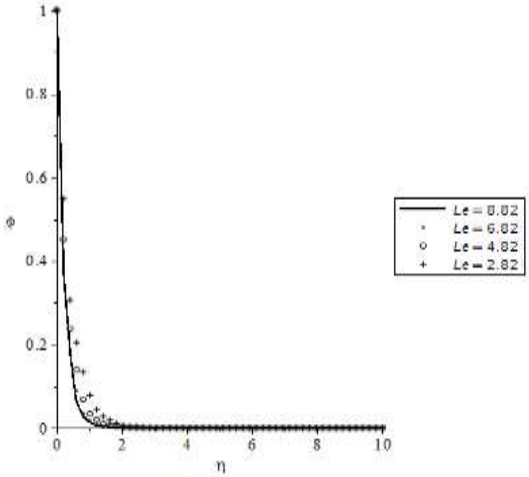

Figure 34: Effects of Le on concentration profile when $n=1,\ Sr=0.1,\ w=0.001,\ \Pr=0.71,\ Kr=2$.

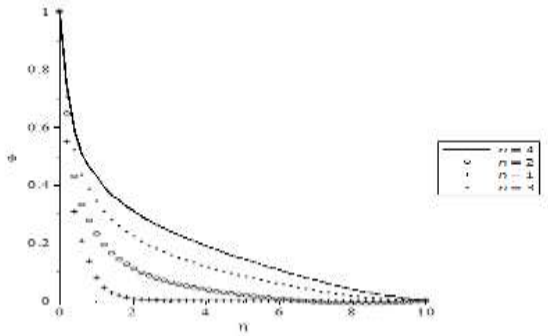

Figure 35: Effects of n on concentration profile when $Sr = 0.1,\ w = 0.001,\ \Pr = 0.71,\ Le = 2.816901,\ Kr = 2$.

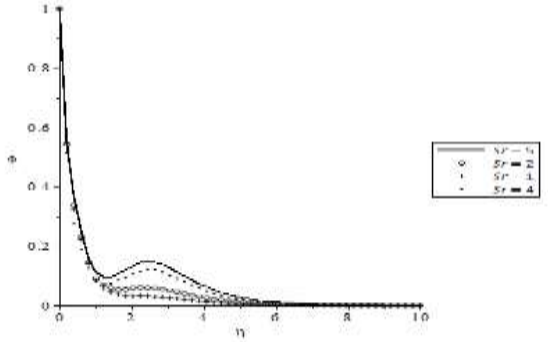

Figure 36: Effects of Sr on concentration profile when $n = 1,\ w = 0.001,\ \Pr = 0.71,\ Le = 2.816901,\ Kr = 2$.

Tables 1-3 show the values of skin-friction coefficients, the local Nusselt and Sherwood numbers, which are respectively proportional to $u'(0)$, $-\theta'(0)$ and $-\phi'(0)$, are sorted out for various values of embedded parameters and presented in tabular form. It should be pointed out that $\lambda > 0$ corresponds to assisting flow (heated plate), $\lambda < 0$ represent the opposing flow and $\lambda = 0$ is the forced convection flow. The analysis for the parametric study reflects that the skin-friction coefficient is enhanced by β, M, n, w, negative values of A, Df, D and Sr while it is depressed by α, Cr, Ec, $\Pr$, λ, Du, positive values of A, Kr, Le and B. It should be noted that the space internal heat source parameter is increasing function of skin-friction coefficient while the temperature-dependent internal heat sink has opposite effect. Furthermore, the values of the local Nusselt number increase with increasing values of β, α, w, Df, λ and Le while the values of the Nusselt number at the surface decrease as M, Rd, Cr, Ec, $\Pr$, n, Pm, Du, Kr and Sr increase. Also, increasing values of β, α, N, λ, w, D, Sr lead to an increase in the local Sherwood number while increasing values of M, Cr, Rd, n, Pm, $\Pr$, Df, Kr and Le correspond to a decrease in the local mass transfer coefficient. It is worth mentioning that higher values of Ec, representing higher viscous dissipation, enhances the local Sherwood number while lower values of Ec depresses it.

Table 1: Numerical computations showing $u'(0)$, $-\theta'(0)$ and $-\phi'(0)$ at $A = -0.2,\ B = -0.4,\ w = 0.001,\ \lambda = 0.2,\ Df = 1.5,\ Le = 2..816901,\ \Pr = 0.71,\ Sr = 3,\ n = 1$:

β	α	M	N	Rd	Cr	Ec	$u'(0)$	$-\theta'(0)$	$-\phi'(0)$
10							0.1548380924276	0.1568246106445	1.845951933633
20							0.1726454632175	0.1532516677967	1.842275171132
35							0.2008593486050	0.1466818118180	1.839094583565
	52						0.1432824551902	0.1516376994845	1.840735887737
	55						0.0948699108485	0.1532596154462	1.842707551792
	60						0.0430246009785	0.1539033647320	1.845945190556
		0.1					0.0192227503586	0.1739573532095	1.847938959478
		0.3					0.0869708842831	0.1647301286919	1.843869630666
		0.4					0.1321349763608	0.1581933673259	1.841677748358

			-5				0.2096332441770	0.1478987769551	1.839786161991
			2				0.1664942063765	0.1504407512536	1.840058776421
			5				0.1478266415272	0.1513309007352	1.840424113350
				1			0.2017490645517	0.1948575130689	1.833371993006
				5			0.1605792192925	0.1016093090118	1.829860699911
				10			0.1206792819718	0.0755875469694	1.822149166859
					0.2		0.1828797493206	0.1369658828355	1.833463758351
					1.0		0.1168689857421	0.0860245342741	1.815671520908
					2.0		0.1044975909015	0.0728238060607	1.814737439611
						0.1	0.2144226403468	0.1703553208112	1.845642501066
						0.3	0.1718296372458	0.1287972632300	1.836448523539
						0.4	0.1551186597188	0.1091256109895	1.835378393328
						0.5	0.1404437278900	0.0897922562303	1.836449515211
						0.7	0.1155763390883	0.0515402402742	1.844572445686
						1.0	0.0859402469430	0.0059801105036	1.870396973518

Table 2: Numerical computations showing $u'(0)$, $-\theta'(0)$ and $-\phi'(0)$ at $\alpha = 50$, $\beta = 30$, $M = 0.5$, $N = -2$, $Rd = 2, Le = 2.112676, Du = 0.1$, $Sr = 3$, $Kr = 2$:

A	Pr	n	w	Pm	B	Df	$u'(0)$	$-\theta'(0)$	$-\phi'(0)$
-0.4							0.1705381126574	0.1468127905324	1.822602287207
-0.2							0.1912380431167	0.1490644855208	1.839804136968
0.05							0.2213013490931	0.1486416907748	1.864610958206
0.1							0.2280253865438	0.1480512960976	1.870066199350
	1						0.1771241919413	0.1341684413683	1.837103457590
	2						0.1399669568836	0.0827784405935	1.838272185483
	3						0.1135231042854	0.0293593409755	1.856181002488
		5					0.4263429040912	0.1375161553947	1.051867835685
		6					0.4522121981763	0.1347548057003	0.975438733897
		7					0.4708862734180	0.1327428975090	0.914075977187
			0.01				0.1675393378290	0.1475730869577	1.766824016728
			0.1				0.1912380431167	0.1490644855208	1.839804136968
			0.2				0.2216066679757	0.1501621483524	1.924388937647
				0.1			0.0147231627116	0.1536662286252	1.848210526581
				0.3			0.0834983895140	0.1534647925981	1.843334525124
				0.4			0.1298101302547	0.1521820948328	1.841193297220
					-0.3		0.1642100542154	0.1125663359829	1.842706389674
					-0.1		0.0758572405069	0.0073505477085	1.867968888777
					0.01		0.0059217736980	0.0922563812959	1.922999473293
					0.08		-0.036145999451	0.1818922657135	1.997791982329
						0.1	-0.067384263243	0.1522643617114	1.856813284422
						0.5	-0.025743860121	0.1535080492915	1.852150471052
						1.0	0.0477872278510	0.1540946391795	1.845692916762

Table 3: Numerical computations showing $u'(0)$, $-\theta'(0)$ and $-\phi'(0)$ at $A = -0.2$, $B = -0.4$, $w = 0.001$, $Ec = 0.2$, $Df = 1.5, M = 0.5$, $\Pr = 0.71$, $Cr = 0.1$, $n = 1$:

λ	Du	Kr	Sr	Le	$u'(0)$	$-\theta'(0)$	$-\phi'(0)$
0.4					0.1233788646109	0.1524186584375	1.841450242829
0.6					0.0733492253809	0.1536233878429	1.843978119888
0.8					0.0328817285997	0.1538132853518	1.846831889322
	0.1				0.1912380431167	0.1490644855208	1.839804136968
	0.2				0.1893012434169	0.1131055347853	1.896823756183
	0.3				0.1873872997649	0.0740957507079	1.961979262770
		1			0.2035549165627	0.1596295755743	1.301852459737
		3			0.1870775402108	0.1405619855273	2.247392011972
		5			0.1837512255589	0.1268289208213	2.890203018451

			0.5		0.1840792128207	0.1501663166688	1.813560940507
			1		0.1855153066701	0.1499528246141	1.818562924006
			5		0.1969250600264	0.1481166146511	1.863241007371
				1.2	1.1786904382962	0.0866715250859	1.428902273743
				1.5	0.4263429040912	0.1375161553947	1.051867835685
				3.0	0.4067459305943	0.1347140312120	1.316824277631

CONCLUSIONS

In this article, an efficient numerical algorithm of midpoint integration scheme enhanced by Richardson's extrapolation has been employed to study the hydromagnetic mixed convection flow, heat and mass transfer of a viscoelastic third grade fluid in a Darcy-Forchheimer porous medium in the presence of thermal radiation, viscous dissipation, non-uniform heat source/sink and chemical reaction of order n. The original partial differential equations for the problem are transformed into a system of coupled ordinary differential equations which is numerically solved. Graphs are plotted to analyze the variations of the pertinent flow parameters including the material parameter for third grade β, material modulus for second grade parameter α, magnetic interaction parameter M, Darcian permeability parameter Pm, Forchheimer parameter Df, dimensionless mixed convection parameter λ, suction velocity parameter S, dimensionless species concentration buoyancy parameter N, thermal radiation parameter Rd, temperature difference parameter Cr, Prandtl number $\Pr$, Eckert number Ec, space dependent internal heat generation/absorption A, temperature dependent internal heat generation/absorption B, Dufour number Du, Schmidt number Sc, rate of chemical reaction parameter Kr, Soret number Sr and order of chemical reaction n.

The presented analysis shows that both temperature and species concentration profiles are appreciably influenced by thermo-diffusion and diffusion-thermo effects. Thermal radiation, magnetic interaction, temperature difference, chemical reaction, Forchheimer, order of chemical reaction, space dependent internal heat source/sink, temperature dependent internal heat source/sink, mixed convection, species concentration buoyancy and the rate of chemical reaction parameters as well as Eckert, Schmidt, Prandtl, Dufour and Soret numbers have noticeable effects on the fluid velocity, temperature and species concentration. It is interesting to note that the emerging parameters have appreciable influences on the skin-friction coefficient, local rates of heat and mass transfer. Finally, the results reveal among others that:

1. The momentum boundary layer thickness increases with an increase in α, B, N, λ, Du and $\Pr$ while it decreases with an increase in β, M, A, Cr, Df, n, Ec and S.
2. The thermal boundary layer thickness decreases with an increase in Rd, α, A, Cr, N and λ but it increases with an increase in β, B, M, Df, n, Ec, Pm and Du.
3. The species concentration boundary layer thickness decreases with an increase in Kr, $\Pr$ and Le while it is an increasing function of Sr.

REFERENCES

Khani, F., Farmany, A., Raji, M.A., Aziz, A. and Samadi, F. (2009). Analytic solution for heat transfer of a third grade viscoelastic fluid in non-Darcy porous media with thermophysical effects. *Communication in Nonlinear Science and Numerical Simulation, 14: 3867-3878.*

Fosdick R.L. and Rajagopal K.R. (1980). Thermodynamics and stability of fluids of third grade. In the Proceedings of the Royal Society of London Ser A, 339: 351-377.

Dunn, E.J. and Rajagopal, K.R. (1995). Fluids of differential type: critical review and thermodynamic Analysis. *International Journal of Engineering Science, 33:689-729.*

Rivlin, R.S. and Ericksen J.L. (1955). Stress- deformation relations for isotropic materials. *Journal of Rational Mechanics and Analysis, 4: 323-425.*

Hayat, T., Abbas, Z., Pop, I, and Asghar S. (2010). Effects of radiation and magnetic field on the mixed convection stagnation-point flow over a vertical stretching sheet in a porous medium. *nternational Journal of Heat and Mass Transfer, 53(1): 466–74.*

Sahoo, B. (2010). Flow and heat transfer of an electrically conducting third grade fluid past an infinite plate with partial slip. *Meccanica, 45(3): 319–330.*

Sahoo, B. and Poncet, S. (2011). Flow and heat transfer of a third grade fluid past an exponentially stretching sheet with partial slip boundary condition. *International Journal of Heat and Mass Transfer, 54(23) :5010–5019.*

Hayat, T., Mustafa, M. and Asghar, S. (2010). Unsteady flow, heat and mass transfer of a third grade fluid over a stretching sheet in the presence of chemical reaction. *Nonlinear Analysis: Real World Applications, 11(14): 3186-3197.*

Hayat, T., Hina, S., Hendi, A.A. and Asghar, S. (2011). Effect of wall properties on the peristaltic flow of a third grade fluid in a curved channel with heat and mass transfer. *International Journal of Heat and Mass Transfer, 54(23-24): 5126-5136.*

Makinde, O.D. and Chinyoka, T. (2011). Numerical study of unsteady hydromagnetic generalized Couette flow of a reactive third-grade fluid with asymmetric convective cooling. *Journal of Computers and Mathematics with Applications, 61: 1167–1179.*

Abbasbandy, S. and Hayat, T. (2011). On series solution for unsteady boundary layer equations in a special third grade fluid. *International Journal of Communications in Nonlinear Science and Numerical Simulation, 16: 3140–3146.*

Aiyesimi, Y.M., Okedayo, G.T. and Lawal, O.W.. (2012). MHD flow of a third grade fluid with heat transfer down an inclined plane. *Mathematical Theory and Modeling, 2(9): 108-119.*

Aziz A, Aziz T (2012). MHD flow of a third grade fluid in porous half space with plate suction or injection: an analytical approach. *Applied Mathematics and Computation, 218(21): 10443–11045.* doi.org/10.1016/j.amc.2012.04.006

Hayat T., Shafiq A., Alsaedi, A., and Awais M. (2013). MHD axisymmetric flow of third grade fluid between stretching sheets with heat transfer. *Computer and Fluids, 86:103–108.*

Hayat T., Iqbal Z., Mustafa M., Hendi A.A. (2013). Melting heat transfer in the stagnation-point flow of third grade fluid past a stretching sheet with viscous dissipation. *Thermal Science, 17: 865-875.*

Baoku, I.G., Olajuwon, B.I. and Mustapha, A.O. (2013). Heat and mass transfer on a MHD third grade fluid with partial slip flow past an infinite vertical insulated porous plate in a porous medium. *International Journal of Heat and Fluid Flow, 40: 81-88.*doi.org/10.1016/j.ijheatfluidflow.2013.01.016

Gul, T., Shah, R.A., Islam, S. and Arif, M. (2013). MHD thin film flows of a third grade fluid on a vertical belt with slip boundary conditions. *Journal of Applied Mathematics Article ID 707286, 14 pages.*doi.org/10.1155/2013/707286 6

Gul, T., Islam, S., Shah, R.A., Khan, I. and Shafie, S. (2014). Thin film flow in MHD third grade fluid on a vertical belt with temperaturedependent viscosity. *PLoS ONE,* 9(6):e97552. doi:10.1371/journal.pone.0097552

Naganthran, K., Nazar, R. and Pop, I. (2016). Unsteady stagnation-point flow and heat transfer of a special third grade fluid past a permeable stretching/shrinking sheet. *Scientific Report, 6: 1-13.* doi: 10.1038/srep24632

Farooq, U., Hayat, T., Alsaedi, A. and Liao, S. (2014). Heat and mass transfer of two-layer flows of third-grade nano-fluids in a vertical channel. *Applied Mathematics and Computation, 242 (1): 528 – 540.*doi: 10.1016/j.amc.2014.05.126

Hayat, T., Shehzad S.A., Qasim, M., Asghar. S. and Alsaedi, A. (2014). Thermally stratified radiative flow of third grade fluid over a stretching surface. *Journal of Thermophysics and Heat Transfer, 28(1): 155–161.* doi: 10.2514/1.T4113

Shehzad S, Hussain T, Hayat T, Ramzan M, Alsaedi A. (2015). Boundary layer f low of third grade nanofluid with Newtonian heating and viscous dissipation. *Journal of Central South University, 22(1):360-367.* doi:10.1007/s11771-015-2530-x

Nadeem, S., Saleem, S. (2015). Analytical study of third grade fluid over a rotating vertical cone in the presence of nanoparticles. *International Journal of Heat and Mass Transfer,85:1041–1048.* doi.org/10.1016/j.ijheatmasstransfer.2015.02.007

Rashidi, M.M., Bagheri, S., Momoniat E. and Freidoonimehr, N. (2015) Entropy analysis of convective MHD flow of third grade non-Newtonian fluid over a stretching sheet. *Ain Shams Engineering Journal, 8 (1):77-85.* doi:10.1016/j.asej.2015.08.012

Hayat T, Shafiq A, Alsaedi A (2015). MHD axisymmetric flow of third grade fluid by a stretching cylinder. *Alexandria Engineering Journal, 54: 205–212.*

Adesanya, S.O. and Falade J.A. (2015). Thermodynamic analysis of hydromagnetic third grade fluid flow through a channel filled with porous medium. *Alexandria Engineering Journal, 54: 615–622.* doi.org/10.1016/j.aej.2015.05.014

Poonia, M. and Bhargava, R. (2015). Heat and mass transfer in unsteady third-grade fluid with variable suction using finite element method. *International Journal of Computational Methods, 12(6): 1550038.* doi: 10.1142/S0219876215500383

Olajuwon, B.I. and Baoku, I.G. (2014). Hydromagnetic partial slip flow, heat and mass transfer of a viscoelastic third grade fluid embedded in a porous medium. *Journal of Nonlinear Studies, 21(3): 387 – 403.*

Abdulhameed M., Varnhorn W., Hasim I. and Roslan, R. (2015). The unsteady flow of a third grade fluid caused by the periodic motion of an infinite wall with transpiration. *Alexandria Engineering Journal, 54(4):1233–1241.* https://doi.org/10.1016/j.aej.2015.06.002

Imtiaz, M., Alsaedi, M., Shafiq, A. and Hayat, T. (2017). Impact of chemical reaction on third grade fluid flow with Cattaneo-Christov heat flux. *Journal of Molecular Liquids, 229: 501 - 507.*doi.org/10.1016/j.molliq.2016.12.103

Hayat, T,. Ahmad, S.M. and Khan, I. and Alsaedi, A. (2018). Modeling and analyzing flow of third grade nanofluid due to rotating stretchable disk with chemical reaction and heat source. *Physica B: Condensed Matter, 573: 116 - 126.* https://doi.org/10.1016/j.physb.2018.01.052

Golafshan, B. and Rahimi, A.B. (2018). Effects of radiation on mixed convection stagnation-point flow of MHD third-grade nanofluid over a vertical stretching sheet. *Journal of Thermal Analysis and Calorimetry, 1 – 17.* doi.org/10.1007/s10973-018-7075-4

Gaffar, S., Prasad, V.R., Beg, O.A., Khan, H.H. and Venkatadri, K. (2018). Radiative and magnetohydrodynamic flow of third-grade viscoelastic fluid past an isothermal inverted cone in the presence of heat generation/absorption. *Journal of the Brazilian Society of Mechanical Sciences and Engineering, 40: 127.* doi.org/10.1007/s40430-018-1049-0

Prasad, K.V., Subhas Abel, M. and Joshi, A. (2000). Oscillatory motion of a viscoelastic fluid over a stretching in a porous media. *Journal of Porous Media, 3(1): 61 - 68.* doi: 10.1615/JPorMedia.v3.i1.50

Sparrow, E. M. and Cess, R.D. (1995). Hemisphere Publ. Stuart- J. T, In Proceeding of Royal Society, Londom A231, 116.

Heck, A. (2003). Introduction to Maple, Third Edition, Springer-Verlag, Germa